Available online at www.sciencedirect.com
SCIENCE DIRECT®
Journal of Hydrology 273 (2003) 69–80
Journal of Hydrology
www.elsevier.com/locate/jhydrol

Simulation of 6-hourly rainfall and temperature by two resampling schemes

R. Wójcik[1], T.A. Buishand*

Royal Netherlands Meteorological Institute (KNMI), P.O. Box 201, 3730 AE De Bilt, The Netherlands

Received 16 November 2001; revised 15 May 2002; accepted 1 November 2002

Abstract

The joint simulation of time series of 6-hourly precipitation and temperature using nearest-neighbour resampling is studied for Maastricht, the Netherlands. Two resampling schemes are considered: (i) straightforward resampling of 6-hourly values, and (ii) resampling of daily values followed by disaggregation into 6-hourly values using the method of fragments. Second-order statistics of the simulated values are compared with those in the observed data. It appeared that straightforward resampling of 6-hourly values does not adequately preserve the slow decay of the autocorrelation functions of precipitation and temperature. As a result the standard deviations of the monthly precipitation totals and monthly average temperature are strongly underestimated. A negative bias also shows up in the quantiles of the multi-day seasonal maximum precipitation amounts. The autocorrelation coefficients and the standard deviations of the monthly values are much better reproduced if the daily values are generated first. A good correspondence between the historical and simulated distributions of the seasonal maximum precipitation amounts is also achieved with this alternative resampling scheme.

Keywords: Rainfall; Temperature; Time correlation; Extreme values; Stochastic rainfall modelling; Disaggregation

1. Introduction

Stochastic rainfall models are a useful tool in the design and evaluation of hydrological systems. A range of methods exists to model rainfall sequences. For a time resolution shorter than a day most models fall into two categories: profile-based and pulse-based. In the profile-based models (e.g. Acreman, 1990; Koutsoyiannis and Pachakis, 1996; Heneker et al., 2001) a storm event is simulated from probability distributions for the inter-arrival time and duration and the conditional distribution of the total depth or mean intensity given the duration. The total depth is then disaggregated into the required time step. In the pulse-based models (e.g. Rodriguez-Iturbe et al., 1987; Cowpertwait et al., 1996; Onof et al., 2000) rain cells arrive in a Poisson-cluster process. This process is either the Bartlett–Lewis or the Neyman–Scott process. Each rain cell is represented as a rectangular pulse of random duration and random intensity. The total storm intensity at any point in time is the sum of the intensities of all active rain cells at that point.

* Corresponding author. Fax: +30-221-0407.
E-mail address: adri.buishand@knmi.nl (T.A. Buishand).
[1] Wageningen University, Department of Environmental Science, Sub-department Water Resources, Nieuwe Kanaal 11, 6709 PA Wageningen, The Netherlands

0022-1694/03/$ - see front matter © 2003 Elsevier Science B.V. All rights reserved.
PII: S0022-1694(02)00355-4

The main advantage of the parametric models above is their flexibility to generate rainfall for a range of time scales and the ability to reproduce relevant statistical characteristics of the original data at a single site. However, hydrological applications often require more input data than just the precipitation for a particular site. Precipitation for several sites and temperature or evapotranspiration may be needed. Multi-site extensions of the profile-based and pulse-based models are not straightforward due to complexity of mathematical description and a need for an extra parametrization. It is also not easy to develop a parametric model for the joint simulation of sub-daily rainfall and other weather variables.

Non-parametric resampling procedures form an alternative to generate artificial records of uni- or multivariate time series of weather variables. Young (1994) proposed nearest-neighbour resampling to simulate daily minimum and maximum temperatures and precipitation. Independently, Lall and Sharma (1996) discussed a nearest-neighbour bootstrap to generate hydrological time series. An application of their algorithm to daily precipitation and five other weather variables was presented in Rajagopalan and Lall (1999). The ability of nearest-neighbour resampling to reproduce several sample statistics and precipitation spell structure was demonstrated. The multi-site simulation of daily rainfall and temperature at 25 stations in the Rhine basin was discussed in Buishand and Brandsma (2001).

The above applications have shown that nearest-neighbour resampling performs well at a daily time scale. None of the research reported in the literature, however, considers this technique for simulating hydrological time series at a finer time scale. In the present paper, we evaluate the performance of nearest-neighbour resampling as a method to generate 6-hourly rainfall and temperature for Maastricht, the Netherlands. This evaluation is part of a study on stochastic weather generation for the Meuse basin. The interest is on the occurrence of high river discharges. Precipitation is the dominant weather variable. Temperature is required to determine snow accumulation and melt and to estimate evapotranspiration. Two resampling schemes are compared: straightforward simulation of 6-hourly values (Scheme 1) and simulation of daily values with disaggregation into 6-hourly values (Scheme 2). As a disaggregation procedure the method of fragments is adapted. For Maastricht, we assess the two resampling schemes in terms of the reproduction of second-order statistics of rainfall and temperature and the distribution of maximum precipitation amounts. The emphasis is on the winter half-year (October–March), because the peak discharges of the Meuse in the Netherlands mainly occur in that period.

2. Nearest-neighbour resampling

In the nearest-neighbour method weather variables like precipitation and temperature are sampled simultaneously with replacement from the historical data. Temporal dependence is incorporated by conditioning on preceding values. For instance, to generate weather variables for a new day $t + 1$, days with similar characteristics as those simulated for the previous day t are firstly selected from the historical record. One of these nearest neighbours is then randomly selected and the observed values for the day subsequent to that nearest neighbour are adopted as the simulated values for day $t + 1$. A feature (or state) vector $\mathbf{D}_t$ is used to find the nearest neighbours in the historical record.

Fig. 1 shows an example of the first five steps of nearest-neighbour resampling in a 3D state space (so $\mathbf{D}_t = [v_1(t), v_2(t), v_3(t)]^T$). The points in the state space (red dots) were obtained by iterating a parametric set of three non-linear state equations described by Pickover (1990). The three state variables in this illustration do not have any particular physical meaning. One could, however, consider them as three relevant weather variables, like e.g. temperature, precipitation and air pressure. To initialize the simulation, one of the historical states is selected at random. This state is depicted in Fig. 1 as a black dot with label 1. Next, the collection of $k = 30$ states (blue dots) which lie closest to the black dot is determined in this example. One of those nearest neighbours (yellow dot) is then selected at random and its successor (a black dot with label 2) is adopted as the simulated state for $t = 2$. Thereafter, again a set of k nearest neighbours is determined, one of them is randomly selected and its successor (black dot with label 3) is delivered as the simulated state for $t = 3$.

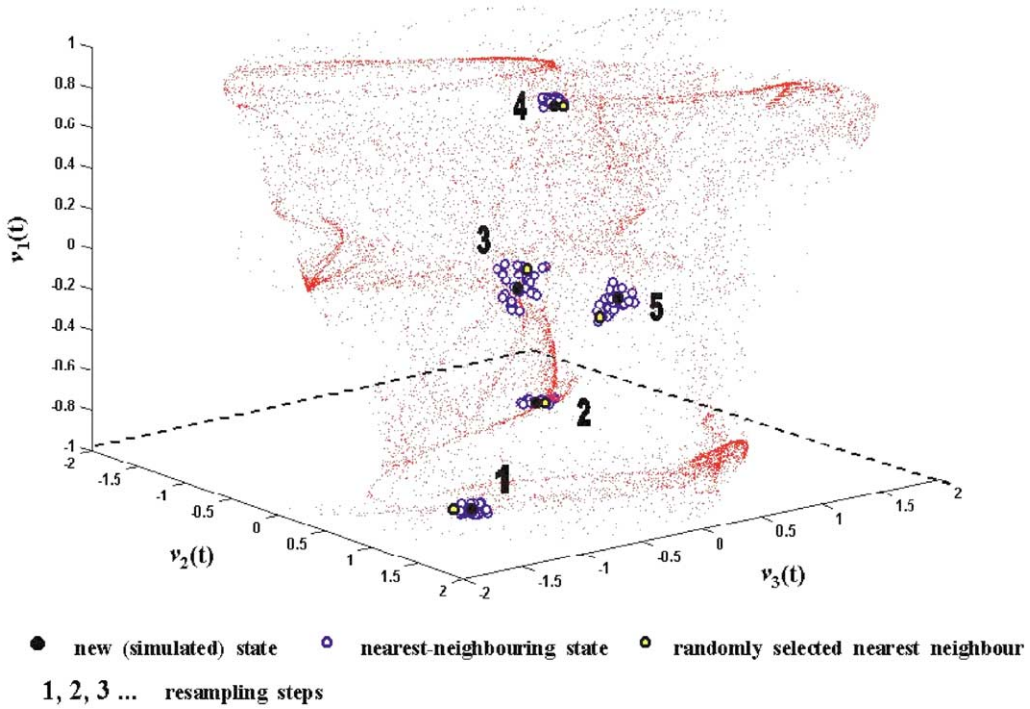

Fig. 1. The principle of nearest-neighbour resampling.

The above procedure is repeated a large number of times.

An important issue in nearest-neighbour resampling is the choice of a function which measures the distance between points in the state space. By using this function (also called a metric) one identifies the k nearest neighbours of a particular state. In this study the *Mahalanobis metric* (e.g. Kendall et al., 1983, p. 290) was used. The Mahalanobis distance between the feature vectors $\mathbf{D}_t$ and $\mathbf{D}_u$ at times t and u is defined as:

$$\delta(\mathbf{D}_t, \mathbf{D}_u) = ((\mathbf{D}_t - \mathbf{D}_u)^T \mathbf{B}^{-1} (\mathbf{D}_t - \mathbf{D}_u))^{1/2} \quad (1)$$

where $\mathbf{B}$ is the covariance matrix of the feature vector $\mathbf{D}_t$. The elements of this matrix are the covariances between the components of $\mathbf{D}_t$:

$$B_{ij} = \mathrm{Cov}(v_i(t), v_j(t)), \qquad i,j = 1,\ldots,q \quad (2)$$

where q is the dimension of $\mathbf{D}_t$.

A discrete probability distribution or kernel is required for resampling from the k nearest neighbours. Lall and Sharma (1996) recommended a kernel that gives higher weight to the closer neighbours. For this decreasing kernel the probability p_n that the nth closest neighbour is resampled is given by:

$$p_n = \frac{1/n}{\sum_{i=1}^{k} 1/i}, \quad n = 1,\ldots,k \quad (3)$$

From the above description it is clear that apart from creating a feature vector, choosing a metric and a probability kernel, the user has to set the number k of nearest neighbours. For the decreasing kernel (Eq. (3)) the reproduction of autocorrelation coefficients gradually deteriorates with increasing k (Buishand and Brandsma, 2001). However, k cannot be taken arbitrarily small. Buishand and Brandsma (2001) have shown that choosing $k = 2$ leads to duplication of large parts of the historical record and to repeated sampling of the same historical values. These phenomena are related to the probabilities p_1 and p_2 and not to the temporal correlation in the data. In accordance with the results in Buishand and Brandsma (2001) we use $k = 5$ in this study.

To reduce the effect of seasonal variation, the search for nearest neighbours was restricted to days within a moving window, centered on the calendar

day of interest. As in Brandsma and Buishand (1998) the width of this window (W_{mw}) was 61 days. Yet another technical issue arises when straightforward simulation of 6-hourly values (Scheme 1) is performed. The search for nearest neighbours has to be further restricted then to the 6-hourly values in a particular section of the day (0–6, 6–12, 12–18 or 18–24 h) in order to preserve the diurnal variation. The resampling procedure runs in that case as follows:

1. Select a day randomly from the days in the moving window centered at day 1. The data of the 0–6 h section of the selected day form the first simulated state.
2. Determine the k nearest neighbours of the simulated state among the values of the first 6 h section of the days in the moving window, using the Mahalanobis distance (Eq. (1)).
3. Sample one of the nearest neighbours in step 2 using the decreasing kernel (Eq. (3)), and adopt its historical successor as the simulated state for the next 6 h interval.
4. Repeat steps 2 (with the search for nearest neighbours in the same day section as that of the simulated state) and 3 until the desired length of record is simulated.

3. Disaggregation by the method of fragments

For the disaggregation of simulated daily rainfall and temperature the method of fragments was adapted. This method is a special case of nearest-neighbour resampling. In order to preserve the dependence between the 6-hourly values at the transition of two days, the selection of a nearest neighbour for the disaggregation of the simulated daily rainfall and temperature data for a particular day t considers both these daily data and the data of the last 6h section of the previous day $t-1$. Maheepala and Perera (1996) modified the method of fragments in a similar way to preserve over-year correlations. Again the Mahalanobis distance is used to identify a nearest neighbour. In Maheepala and Perera (1996) the selection of a nearest neighbour was based on a scaled Euclidean distance.

For a mathematical description of the selection process the following vector pairs are defined:

$$\mathbf{X}_t^* = [x_1^*(t), x_2^*(t), \ldots, x_n^*(t)]^T$$
$$\mathbf{X}_u = [x_1(u), x_2(u), \ldots, x_n(u)]^T \tag{4}$$

and

$$\mathbf{\Phi}_{t-1}^* = [\phi_1^*(t-1), \phi_2^*(t-1), \ldots, \phi_n^*(t-1)]^T$$
$$\mathbf{\Phi}_{u-1} = [\phi_1(u-1), \phi_2(u-1), \ldots, \phi_n(u-1)]^T \tag{5}$$

where $x_i^*(t)$ is the simulated daily value of the ith weather variable ($i = 1, \ldots, n$) for day t, $x_i(u)$ is the daily value obtained by summing (for rainfall) or averaging (for temperature) 6-hourly values of the ith weather variable for day u in the historical record, $\phi_i^*(t-1)$ is the value of the ith weather variable simulated for the last 6h section of day $t-1$ and $\phi_i(u-1)$ is the value of the ith weather variable in the last 6 h section of day $u-1$ in the historical record. In this study $n = 2$ since rainfall and temperature are the only weather variables. For each day t in the simulated sequence, the distances:

$$\alpha_u = ((\mathbf{X}_t^* - \mathbf{X}_u)^T \mathbf{C}^{-1} (\mathbf{X}_t^* - \mathbf{X}_u))^{1/2} \tag{6}$$

$$\beta_u = ((\mathbf{\Phi}_{t-1}^* - \mathbf{\Phi}_{u-1})^T \mathbf{G}^{-1} (\mathbf{\Phi}_{t-1}^* - \mathbf{\Phi}_{u-1}))^{1/2} \tag{7}$$

are calculated for all days u in the historical record falling within a moving window of width $W_{mw} = 61$. The matrices $\mathbf{C}$ and $\mathbf{G}$ are the covariance matrices of $\mathbf{X}_u$ and $\mathbf{\Phi}_{u-1}$, respectively, defined analogous to Eq. (2). Then the day v is found such that:

$$\alpha_v + \beta_v = \min_u (\alpha_u + \beta_u) \tag{8}$$

Day v is thus the day in the historical record for which the weather situation is closest to that simulated for day t and is therefore used for disaggregation.

For precipitation the ratios of the 6h values ('the fragments') to the total amount of day v are used to disaggregate the simulated value P_t^* for day t. The disaggregated rainfall amounts $P_{t,l}^*$ for the 6h sections of day t are then given by:

$$P_{t,l}^* = w_{v,l} P_t^*, \quad l = 1, \ldots, 4 \tag{9}$$

where:

$$w_{v,l} = \frac{P_{v,l}}{\sum_{l=1}^{4} P_{v,l}} \tag{10}$$

where $P_{v,l}$ is the 6-hourly rainfall amount for the lth section of day v. In order to preserve the daily mean temperature the following additive structure is used:

$$T^*_{t,l} = T_{v,l} + \bar{T}^*_t - \bar{T}_v \tag{11}$$

where $T^*_{t,l}$ is the disaggregated temperature for the lth section of day t, $T_{v,l}$ is the temperature for the lth section of the selected historical day v, $\bar{T}^*_t$ is the simulated temperature for day t and

$$\bar{T}_v = \frac{1}{4}\sum_{l=1}^{4} T_{v,l} \tag{12}$$

A stochastic variant of the above method is easily obtained by searching for the k days with smallest $(\alpha_u + \beta_u)$ and selecting one at random using the discrete probability kernel (Eq. (3)).

4. Data description and pre-processing

The rainfall and temperature data used were recorded at the airport of Maastricht, the Netherlands (latitude 50.92°N, longitude 5.78°E, altitude 114 m) for 42 years (1958–1999). The mean annual rainfall at this site is 760 mm. The Maastricht record is the longest record of sub-daily weather variables in the Meuse basin. The measurements were originally archived with a time resolution of 1 h. The precipitation records were aggregated and temperature records were averaged to obtain the data with 6-hourly and daily resolution. The original 1 h resolution was judged to be too fine for runoff modelling in the Meuse basin.

Before resampling the data were standardised. This further reduces the effect of seasonal variation. The daily temperature was standardised by subtracting an estimate m_d of the mean and dividing by an estimate s_d of the standard deviation for the calendar day d of interest:

$$\tilde{x}_u = (x_u - m_d)/s_d, \quad u = 1, \ldots, 365J; \text{ and}$$

$$d = (u-1)\bmod 365 + 1 \tag{13}$$

where x_u and $\tilde{x}_u$ are the original and standardised variables for day u, respectively, and $J = 42$ is the total number of years in the record. The estimates m_d and s_d were obtained by smoothing the sample mean and standard deviation for the successive calendar days using the Nadaraya–Watson smoother (for more details see, e.g. Hastie and Tibshirani, 1990, p.19). The smoothed statistic $g(d)$ for day d is given by:

$$g(d) = \frac{\sum_{\varphi=d-\sigma}^{d+\sigma} \kappa\left(\frac{d-\varphi}{\sigma}\right) z_\varphi}{\sum_{\varphi=d-\sigma}^{d+\sigma} \kappa\left(\frac{d-\varphi}{\sigma}\right)}, \quad d = 1, \ldots, 365 \tag{14}$$

where z_φ is the raw value of the statistic for calendar day φ, $\kappa(\cdot)$ is a kernel function and σ is the bandwidth[2]. In this study the Epanechnikov kernel was applied:

$$\kappa(a) = \begin{cases} \frac{3}{4}(1-a^2), & \text{for } |a| \le 1 \\ 0 & \text{otherwise} \end{cases} \tag{15}$$

where $a = (d-\varphi)/\sigma$. The bandwidth σ was set to 30 days for temperature and 45 days for precipitation. Daily precipitation was standardised by dividing by a smooth estimate $m_{d,\text{wet}}$ of the mean wet-day precipitation amount:

$$\tilde{x}_u = x_u/m_{d,\text{wet}}, \quad u = 1, \ldots, 365J; \text{ and}$$

$$d = (u-1)\bmod 365 + 1 \tag{16}$$

A wet day was defined here as a day with $P \ge 0.1$ mm. Fig. 2 shows the values of m_d and s_d for T and $m_{d,\text{wet}}$ for P, together with their smoothed approximations. Particularly in the latter two statistics there are large day-to-day fluctuations due to sampling effects.

[2] To apply Eq. (14) the values z_φ for $\varphi = 366-\sigma, \ldots, 365$ were inserted for $\varphi = 1-\sigma, \ldots, 0$ and the values z_φ for $\varphi = 1, \ldots, \sigma$ were inserted for $\varphi = 366, \ldots 365+\sigma$.

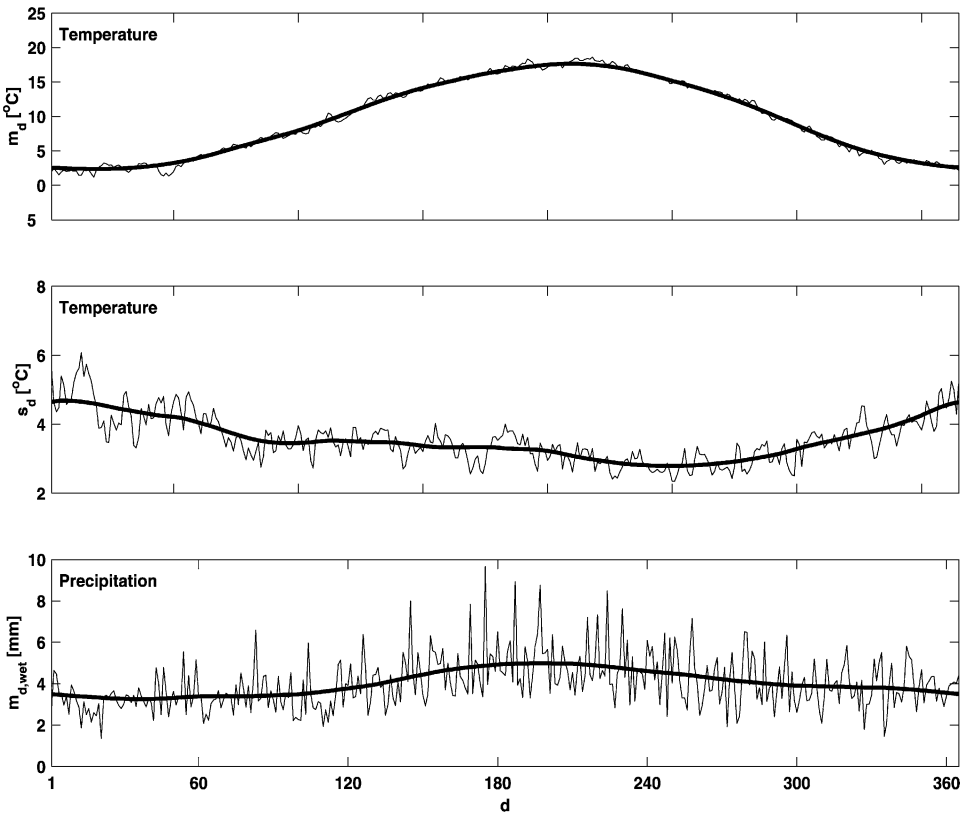

Fig. 2. Values of m_d and s_d for daily temperature (T) and $m_{d,\mathrm{wet}}$ for daily precipitation (P) in Maastricht together with their smoothed approximations as a function of calendar day d for the period 1957–1998. The smooth curves are computed using the Nadaraya–Watson estimator with the Epanechnikov kernel.

The standardisation does not reduce the seasonal variation in rainfall occurrence. It also does not affect the seasonally varying dependence between precipitation and temperature. The use of a moving window remains therefore necessary. However, its width can be broader if part of the seasonal variation is removed prior to resampling. For 6-hourly temperature and precipitation Eqs. (13) and (16) were applied to each 6 h section of the day separately.

5. Model identification

Precipitation and temperature data were generated with two different temporal resolutions: 6-hourly and daily. In both cases a first-order resampling model was applied. This implies that the feature vector $\mathbf{D}_t$ comprises rainfall and temperature generated for the previous 6 hours or the previous day (depending on the time resolution considered). Additionally, for 6-hourly simulations the inclusion of generated variables for the two previous 6-hourly time steps was studied (second-order model). The Mahalanobis distance was incorporated in all simulation models. The covariance matrix $\mathbf{B}$ defined by Eq. (2) was calculated in two ways:

- globally for the entire set of standardised weather variables (for 6-hourly values for each 6 h section of the day separately), yielding the global covariance (GC) model
- locally, i.e. using only the values of the standardised weather variables lying within the moving data window (and for 6-hourly values also within a particular day section), yielding the local covariance (LC) model, respectively

The LC model is computationally more expensive, however, it accounts for seasonal variation in the covariances between rainfall and temperature. These covariances are negative in summer and positive in winter. For the second-order models the LC scheme also accounts for the seasonal variation of the lag 1 autocovariances of rainfall and temperature. To disaggregate simulated daily values of precipitation and temperature, the nearest-neighbour search was conducted using Eqs. (6) and (7) where the matrices **C** and **G** were computed according to the GC and LC schemes. The GC scheme was used if the daily simulations were done with a GC model and the LC scheme was used if the daily simulations were done with an LC model. These models are referred to as DISGC and DISLC.

6. Results

6.1. Reproduction of standard deviations and autocorrelation

The performance of the models was first assessed in terms of the reproduction of the standard deviations of the 6-hourly temperature and precipitation, the standard deviations of the monthly average temperature and the monthly precipitation totals, and the 6-hourly autocorrelation coefficients for the winter half-year (October–March). To reduce the influence of the annual cycle the above statistics were first calculated for each calendar month separately. The effect of the diurnal cycle was accounted for by using separate values for the mean of each day section in the calculation of the 6-hourly autocovariances. Thus, given N values $x_1, x_2, \ldots, x_N$ (of precipitation or temperature) in a particular month, the lag τ autocovariance was estimated as:

$$c(\tau) = \frac{1}{N}\sum_{i=1}^{N-\tau}(x_i - \bar{x}_{(i-1)\bmod 4+1}) \times (x_{i+\tau} - \bar{x}_{(i+\tau-1)\bmod 4+1}) \quad (17)$$

with $\bar{x}_1, \bar{x}_2, \bar{x}_3$ and $\bar{x}_4$ being the averages for the four day sections. The lag τ autocorrelation coefficient was then estimated as:

$$r(\tau) = c(\tau)/c(0) \quad (18)$$

where $c(0) = s_{6h}^2$ is the variance. For each of the analyzed weather variables the winter estimates were obtained by taking the arithmetic mean of the monthly estimates over the six winter months (October–March).

A run of 420 years was generated to investigate the performance of the two resampling schemes. A rather long simulation run was considered to reduce the standard errors of the second-order statistics. These statistics were estimated in the same way as for the historical data. The average estimates $\bar{s}_{6h}^*$, $\bar{s}_M^*$, $\bar{r}^*(\tau)$ of the standard deviations of the 6-hourly and monthly values and the lag τ autocorrelation coefficient, respectively, were compared with the estimates $\bar{s}_{6h}$, $\bar{s}_M$, $\bar{r}(\tau)$ for the historical data. The relative difference $\Delta\bar{s}_{6h}$ between the observed and simulated 6-hourly standard deviation was calculated using:

$$\Delta\bar{s}_{6h} = (\bar{s}_{6h}^* - \bar{s}_{6h})/\bar{s}_{6h}\ 100\% \quad (19)$$

with a similar equation for the relative difference $\Delta\overline{SM}$ of the standard deviation of the monthly values, and

$$\Delta\bar{r}(\tau) = [\bar{r}^*(\tau) - \bar{r}(\tau)], \quad \tau = 1, 2, 3, \ldots \quad (20)$$

for the difference $\Delta\bar{r}(\tau)$ of the lag τ autocorrelation coefficient. In order to evaluate the statistical significance of $\Delta\bar{s}_{6h}$, $\Delta\bar{s}_M$ and $\Delta\bar{r}(\tau)$ standard errors *se* were calculated for the estimates from the historical record. The standard errors were obtained with the jackknife method in Buishand and Beersma (1996). A criterion of $2 \times se$ was used to indicate significant differences between the historical and simulated values. This roughly corresponds to a two-sided test at the 5% level (Brandsma and Buishand, 1998).

Table 1 presents $\Delta\bar{s}_{6h}$, $\Delta\bar{s}_M$, and $\Delta\bar{r}(\tau)$ for resampling Scheme 1. Instead of presenting $\Delta\bar{r}(3)$, $\Delta\bar{r}(4)$, $\Delta\bar{r}(5)$ separately, the average difference $\overline{\Delta\bar{r}(3,4,5)}$ taken over these three lags is shown.

For the first-order 6 h resampling models (GC1, LC1), Table 1 shows that a number of statistics are not well reproduced. A large and statistically significant negative bias is present in the standard deviations of monthly rainfall and temperature. This bias is caused by a strong underestimation of the higher order autocorrelation coefficients. For precipitation large

Table 1
Performance of the direct simulation of 6-hourly values (Scheme 1; one run for 420 years for each case) for the winter (October–March). For each statistic the differences (mean precipitation in mm, mean temperature in °C and autocorrelation coefficients, dimensionless) or percentage differences (standard deviations) are given between the simulated and historical data (1958–1999). The historical values of the mean and standard deviations in the bottom line are in mm (precipitation) or °C (temperature)

Case	Mean		$\Delta\bar{s}_M$		$\Delta\bar{s}_{6h}$		$\Delta\bar{r}(1)$		$\Delta\bar{r}(2)$		$\overline{\Delta\bar{r}(3,4,5)}$	
	P	*T*	*P*	*T*	*P*	*T*	*P*	*T*	*P*	*T*	*P*	*T*
GC1	−15.0	0.0	−15.3[a]	−9.8[a]	−0.9	−0.2	−0.010	−0.003	0.008	−0.009	−0.034[a]	0.007
LC1	−17.4	0.0	−15.7[a]	−8.9[a]	−1.7	−0.3	−0.006	−0.003	−0.007	0.009	−0.035[a]	0.008
GC2	−40.2[a]	0.4[a]	−19.9[a]	−25.2[a]	−3.3	−6.5[a]	−0.011	−0.022[a]	−0.007	−0.040[a]	−0.039[a]	−0.074[a]
LC2	−69.0[a]	0.2	−23.8[a]	−23.9[a]	−6.6[a]	−4.8[a]	−0.006	−0.021[a]	−0.006	−0.039[a]	−0.040[a]	−0.075[a]
Historical	377.4	5.0	31.2	2.1	1.5	4.3	0.354	0.927	0.164	0.837	0.095	0.750

[a] Value differs more than 2 × *se* from the estimate for the historical data.

biases are found for $\tau = 3, 4$ and 5, whereas for temperature the largest biases occur at higher lags. The first-order models are simply not able to deal with the slow decay of the autocorrelation function in the 6-h rainfall and temperature data. This also applies to the second-order models (GC2, LC2). Moreover, the simulations with those models suffer from a significant underestimation of the seasonal mean rainfall.

Table 2 displays the results for resampling Scheme 2. For the 6h disaggregated rainfall, the bias in the higher order autocorrelation coefficients is much smaller than that in Table 1. In consequence, $\bar{s}_M$ is much better reproduced than in the straightforward 6 h simulations. For the same reason the underestimation of the standard deviations of monthly temperatures is much smaller than in resampling Scheme 1.

Furthermore, Tables 1 and 2 demonstrate that the way the covariance matrices are computed has little impact on the performance of the simulation procedure. Simplifications are thus conceivable.

Table 3 compares the two resampling schemes for the summer half-year (April–October). Despite the differences in precipitation regime between winter (mainly widespread frontal rain) and summer (more convective precipitation) the results are quite similar for the two seasons. The direct 6 h simulations (LC1, GC2) in Table 3 show statistically significant biases in the higher order autocorrelation coefficients ($\tau > 2$) of precipitation and temperature as well as in the standard deviations of the monthly values. The use of the second-order GC2 model results again in a significant underestimation of the seasonal mean rainfall. The biases are strongly reduced in the DISLC simulation.

The disaggregation of the daily values in Scheme 2 was also done with the randomized version of the method of fragments in Section 3. This gave almost identical results to those in Tables 2 and 3.

Table 2
Performance of the simulation of daily values followed by disaggregation into 6-hourly values (Scheme 2; one run of 420 years for each case) for the winter (October–March). For each statistic the differences (mean precipitation in mm, mean temperature in °C and autocorrelation coefficients, dimensionless) or percentage differences (standard deviations) are given between the simulated and historical data (1958–1999). The historical values of the mean and standard deviations in the bottom line are in mm (precipitation) or °C (temperature)

Case	Mean		$\Delta\bar{s}_M$		$\Delta\bar{s}_{6h}$		$\Delta\bar{r}(1)$		$\Delta\bar{r}(2)$		$\overline{\Delta\bar{r}(3,4,5)}$	
	P	*T*	*P*	*T*	*P*	*T*	*P*	*T*	*P*	*T*	*P*	*T*
DISGC	−10.2	0.1	−4.0	−3.2	−0.5	−1.4	−0.027[a]	−0.011[a]	−0.014	−0.015[a]	−0.002	−0.028[a]
DISLC	−19.8	0.0	−5.3	−3.6	−1.9	−0.5	−0.018	−0.010[a]	−0.011	−0.013	−0.001	−0.029[a]
Historical	377.4	5.0	31.2	2.1	1.5	4.3	0.354	0.927	0.164	0.837	0.095	0.750

[a] Value differs more than 2 × *se* from the estimate for the historical data.

Table 3
Performance of the simulation of 6-hourly values for the summer (April–September). The cases LC1 and GC2 refer to direct simulation and DISLC to simulation of daily values followed by disaggregation into 6-hourly values (one run of 420 years for each case). For each statistic the differences (mean precipitation in mm, mean temperature in °C and autocorrelation coefficients, dimensionless) or percentage differences (standard deviations) are given between the simulated and historical data (1958–1999). The historical values of the mean and standard deviations in the bottom line are in mm (precipitation) or °C (temperature)

Case	Mean		$\Delta\overline{S}_M$		$\Delta\overline{s}_{6h}$		$\Delta\overline{r}(1)$		$\Delta\overline{r}(2)$		$\Delta\overline{r}(3,4,5)$	
	P	*T*	*P*	*T*	*P*	*T*	*P*	*T*	*P*	*T*	*P*	*T*
LC1	3.0	0.0	−19.3[a]	−13.5[a]	0.3	0.3	0.006	−0.001	0.003	0.004	−0.030[a]	−0.076[a]
GC2	−40.8[a]	0.3	−21.3[a]	−17.1[a]	−4.0	−0.6	−0.012	−0.012[a]	−0.005	−0.019[a]	−0.021[a]	−0.066[a]
DISLC	2.4	0.0	−8.4	1.2	0.6	1.2	−0.022	0.004	−0.003	0.025[a]	−0.005	−0.021[a]
Historical	386.4	16.3	34.1	1.4	1.9	3.6	0.237	0.851	0.083	0.705	0.050	0.656

[a] Value differs more than $2 \times se$ from the estimate for the historical data.

6.2. Maximum precipitation amounts

A number of 1000-year simulations were performed. For three of these simulations (LC1, GC2 and DISLC) Fig. 3 shows Gumbel plots of the 6-h, 1-,4- and 10-day winter precipitation maxima. In the case of 6 h maxima, the greater part of the simulated curves lies close to the curve for the historical data. However, the simulated curves show a tendency towards flattening at a level much higher than the maximum historical precipitation. For the LC1 and GC2 simulations this level corresponds to the value of an extremely large 6 h precipitation amount just outside the boundary of the winter half-year. This precipitation amount can, however, be resampled on days within the winter half-year as a result of the use of the moving window. In resampling Scheme 2 an extremely large 6-hourly precipitation amount is created if a large daily amount is resampled (possibly from outside the winter half-year) and then disaggregated using a historical day with very high precipitation in one of the 6 h sections.

For 4- and 10-day precipitation, only the DISLC model from Scheme 2 is able to reproduce the distribution of the historical data properly. The curves for the LC1 and GC2 simulations in Fig. 3, lie below the curve for the historical data. This striking bias in the quantiles of the extreme multi-day precipitation amounts is mainly due to the poor reproduction of the autocorrelation function. Because of the negative bias in the higher order autocorrelation coefficients the standard deviations of the simulated 4- and 10-day precipitation amounts will be too low, implying that the probability distribution is too much concentrated around the mean. Large precipitation amounts therefore occur less often than they should. Especially for the GC2 simulation the underestimation of the mean and standard deviation of the 6 h values also contributes to the bias in the quantiles of the 4- and 10-day extremes. Both the highest 4-day and 10-day precipitation amounts in the DISLC simulation largely exceed the highest observed values. These maxima lie almost on the straight line representing the Gumbel distribution.

The first 840 years of each simulation run was split into 20 runs of 42 years to assess the statistical significance of the observed differences between the historical and simulated maxima. Fig. 4 shows the results for the 4-day winter maxima in the LC1 and DISLC simulations. The dash-dotted lines in the figure represent the smallest and largest values in the 20 simulation runs. These envelopes may be regarded as approximate 90% confidence bands for the 4-day maximum distribution in a 42-year period. The plot for the historical data is entirely within the envelopes for the DISLC simulation but not within those for the LC1 simulation. So there is some statistical evidence of a systematic departure of the historical 4-day maximum distribution from that in the LC1 simulation. The large variability of the maxima makes it more difficult to find deficiencies of a resampling procedure in an extreme-value distribution than in the second-order statistics of the 6h precipitation amounts.

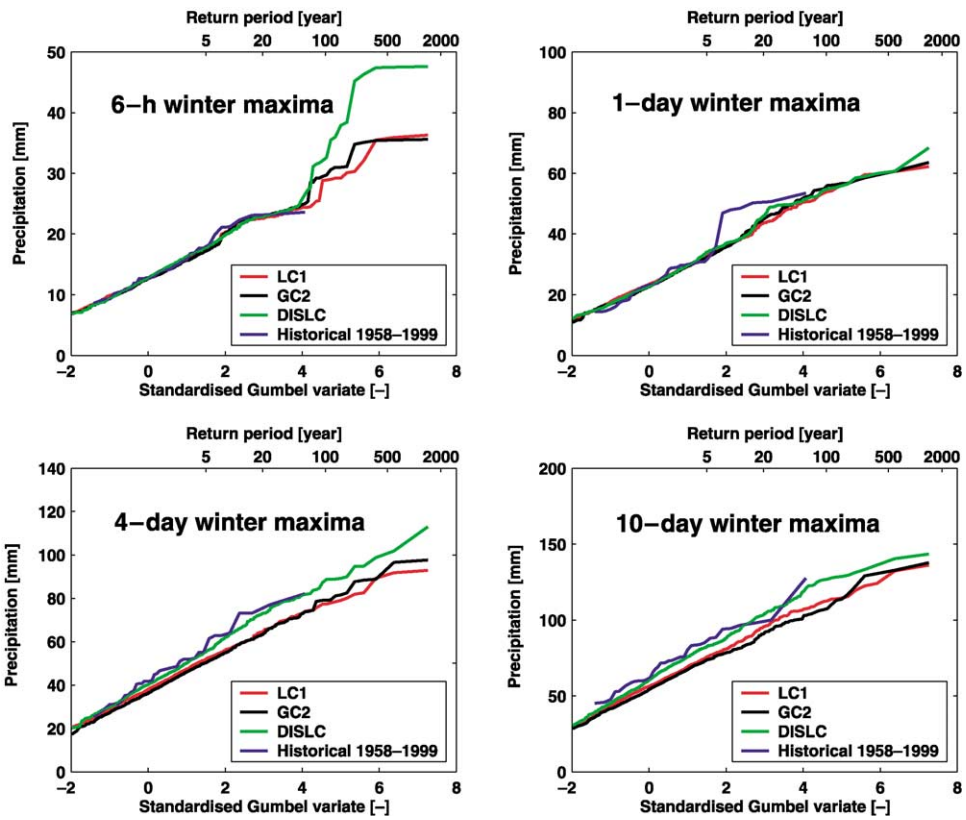

Fig. 3. Gumbel plots of 6-h, 1-,4- and 10-day winter precipitation maxima for historical and simulated data (runs of 1000 years).

The results for the summer half-year are quite similar. For return periods in excess of about 10 years, the quantiles of the 4- and 10-day summer maxima are considerably underestimated in the LC1 and GC2 simulations. The DISLC simulation does much better for these extremes. The distribution of the 4- and 10-day summer maximum precipitation amounts in that simulation is close to the Gumbel distribution.

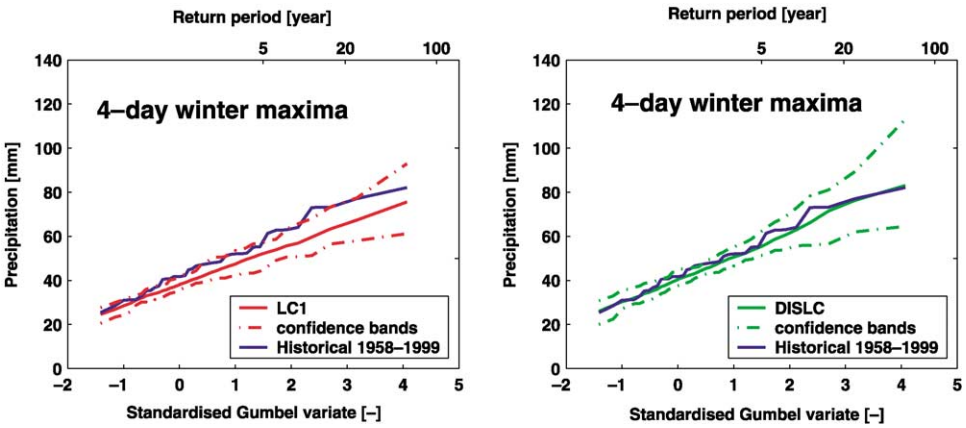

Fig. 4. Gumbel plots of 4-day winter precipitation maxima for historical and simulated data. The dash-dotted lines represent the envelopes of 20 simulation runs of 42 years and the solid line is the average plot for these runs.

Like for the winter half-year, the most extreme simulated values are well above the highest observed values.

7. Discussion and conclusions

In this paper two resampling schemes for the simulation of 6-hourly rainfall and temperature were compared. The simulations using Scheme 1 did not preserve a number of second-order statistics of observed rainfall and temperature properly. Particularly the standard deviations of monthly values were significantly underestimated. This negative bias was mainly due to the inability to reproduce the slow decay of the autocorrelation function of 6-h rainfall and temperature. Introduction of second-order models to tackle this problem remained without success. Because of the above deficiency the quantiles of the simulated 4- and 10-day maximum precipitation amounts were lower than those in the historical record.

More optimistic results were obtained with resampling Scheme 2. Both for rainfall and temperature the second-order statistics were reproduced much better than in Scheme 1. Moreover, the distributions of the simulated rainfall maxima were quite close to those from the historical record. A single simulation run of 1000 years demonstrated that for longer durations (4 and 10 days) the generated maxima follow the Gumbel distribution, also outside the range of the historical data.

The application of stochastic weather simulation to large river basins like the Meuse basin requires a multi-site extension. Multi-site simulation of daily precipitation and temperature in the adjacent Rhine basin using nearest-neighbour resampling is discussed in Buishand and Brandsma (2001). Because the observed weather of historical days is resampled this technique automatically preserves the spatial dependence of the daily rainfall amounts and daily temperatures. This in contrast with approaches based on the multivariate normal distribution (Wilks, 1999; Bárdossy and Van Mierlo, 2000). The use of the method of fragments for the temporal disaggregation of multi-site weather data requires further study. Preliminary results for a subbasin of the river Meuse look promising (Wójcik and Buishand, 2001).

A limitation of a resampling technique is that the simulated values cannot be larger than the highest observed value. The fact that the most extreme simulated multi-day precipitation amounts exceed the highest observed values is purely due to a reshuffling of the historical days with heavy precipitation.

Tables 2 and 3 show that also in Scheme 2 the standard deviation of the monthly totals is underestimated, in particular in the summer half-year. A similar bias was observed in earlier studies on nearest-neighbour resampling (Brandsma and Buishand, 1998; Buishand and Brandsma, 2001). Especially for drought studies it may be useful to incorporate long-term dependence. This can be achieved by including variables in the feature vector that characterise low-frequency variability (Harrold et al., 2001).

Summarizing, it is clear that this study revealed a serious flaw of nearest-neighbour resampling as a method to straightforwardly generate rainfall and temperature with a temporal resolution of 6 h. This technique, however, performs much better at a daily time scale so it is possible to combine it with a disaggregation procedure to obtain the required finer scale (6-hourly) values as demonstrated with Scheme 2.

Acknowledgements

The authors wish to thank Prof. A. Bārdossy and an anonymous reviewer for their comments on an earlier version of the paper. The work was performed in co-operation with the Institute for Inland Water Management and Waste Water Treatment (RIZA) as part of a larger study on stochastic weather generation for the Meuse basin.

References

Acreman, M.C., 1990. A simple stochastic model of hourly rainfall for Farnborough, England. Hydrological Sciences Journal 35, 119–148.

Bārdossy, A., Van Mierlo, J.M.C., 2000. Regional precipitation and temperature scenarios for climate change. Hydrological Sciences Journal 45, 559–575.

Brandsma, T., Buishand, T.A., 1998. Simulation of extreme precipitation in the Rhine basin by nearest-neighbour resampling. Hydrology and Earth System Sciences 2, 195–209. Errata, 3, p.319.

Buishand, T.A., Beersma, J.J., 1996. Statistical tests for comparison of daily variability in observed and simulated climates. Journal of Climate 9, 2538–2550. Errata, 10, p. 818.

Buishand, T.A., Brandsma, T., 2001. Multi-site simulation of daily precipitation and temperature in the Rhine basin by nearest-neighbour resampling. Water Resources Research 37, 2761–2776.

Cowpertwait, P.S.P., O'Connell, P.E., Metcalfe, A.V., Mawdsley, J.A., 1996. Stochastic point process modelling of rainfall. I. Single site fitting and validation. Journal of Hydrology 175, 17–46.

Harrold, T.I., Sharma, A., Sheather, S.J., 2001. Stochastic generation of daily rainfall occurrence: 2. A nonparametric simulation model. Submitted for publication.

Hastie, T.J., Tibshirani, R.J., 1990. Generalized Additive Models, Chapman and Hall, London.

Heneker, T.M., Lambert, M.F., Kuczera, G., 2001. A point rainfall model for risk-based design. Journal of Hydrology 247, 54–71.

Kendall, M., Stuart, A., Ord, J.K., 1983. The Advanced Theory of Statistics, Vol. 3: Design and Analysis, and Time Series, Charles Griffin, London.

Koutsoyiannis, D., Pachakis, D., 1996. Deterministic chaos vs. stochasticity in analysis and modelling of point rainfall series. Journal of Geophysical Research 101, 26441–26451.

Lall, U., Sharma, A., 1996. A nearest neighbor bootstrap for resampling hydrologic time series. Water Resources Research 32, 679–693.

Maheepala, S., Perera, B.J.C., 1996. Monthly hydrologic data generation by disaggregation. Journal of Hydrology 178, 277–291.

Onof, C., Chandler, R.E., Kakou, A., Northrop, P., Wheater, H.S., Isham, V., 2000. Rainfall modelling using Poisson-cluster processes: a review of developments. Stochastic Environmental Research and Risk Assessment 14, 384–411.

Pickover, C., 1990. Computers, Pattern, Chaos and Beauty: Graphics from an Unseen World, St. Martin's Press, New York.

Rajagopalan, B., Lall, U., 1999. A k-nearest-neighbor simulator for daily precipitation and other variables. Water Resources Research 35, 3089–3101.

Rodriguez-Iturbe, I., Cox, D.R., Isham, V., 1987. Some models for rainfall based on stochastic point processes. Proceedings of the Royal Society London, A 410, 269–288.

Wilks, D.S., 1999. Simultaneous stochastic simulation of daily precipitation, temperature and solar radiation at multiple sites in complex terrain. Agricultural and Forest Meteorology 96, 85–101.

Wójcik, R., Buishand, T.A., 2001. Rainfall generator for the Meuse basin: Simulation of 6-hourly rainfall and temperature for the Ourthe catchment. KNMI-publication 196-I, Royal Netherlands Meteorological Institute, De Bilt.

Young, K.C., 1994. A multivariate chain model for simulating climatic parameters from daily data. Journal of Applied Meteorology 33, 661–671.